Negative refraction of Lamb modes: A theoretical study

François Legrand, Benoît Gérardin, Jérôme Laurent, Claire Prada, and Alexandre Aubry
ESPCI Paris, CNRS, PSL University, Institut Langevin, UMR 7587, 1 Rue Jussieu, F-75005 Paris, France

(Received 15 June 2018; revised manuscript received 28 November 2018; published 26 December 2018)

This paper provides a theoretical investigation of negative refraction and focusing of elastic guided waves in a freestanding plate with a steplike thickness change. Under certain conditions, a positive phase velocity (forward) Lamb mode can be converted into a negative phase velocity (backward) mode at such interface, giving rise to negative refraction. A semianalytical model is developed to study the influence of various parameters such as the material Poisson's coefficient, the steplike thickness, the frequency, and the incidence angle. To this end, all the Lamb and shear horizontal propagating modes and also a large number of their inhomogeneous and evanescent counterparts are taken into account. The boundary conditions applied to the stress-displacement fields at the thickness step yields an equation system. Its inversion provides the transmission and reflection coefficients between each mode at the interface. The steplike thickness and Poisson's ratio are shown to be key parameters to optimize the negative refraction process. In terms of material, Duralumin is found to be optimal as it leads to a nearly perfect conversion between forward and backward modes over broad frequency and angular ranges. An excellent focusing ability is thus predicted for a flat lens made of two symmetric thickness steps. A laser ultrasonic experiment quantitatively confirms those theoretical predictions. This study paves the way toward the optimization of elastic devices based on negative refraction, in particular for cloaking or superfocusing purposes.

DOI: 10.1103/PhysRevB.98.214114

I. INTRODUCTION

Negative refraction (NR) has drawn considerable attention for the last 20 years, whether it be for wave focusing [1], lensing [2], imaging [3], or cloaking [4] purposes. In a negative index material, the energy flow as dictated by the Poynting vector is in the opposite direction to the wave vector [2]. This peculiar property implies that, at an interface between positive and negative index material, waves are bent the unusual way relative to the normal. Any negative refracting slab thus forms a flat lens which does not suffer from any spherical aberration [1]. Negative refraction has also given rise to the notion of complementary media and the ability to cancel the propagation of waves by adjoining two mirror regions of opposite refractive indices [5].

Most experiments on negative refraction of elastic waves have been achieved either using phononic crystals [6–9] or metamaterials [10], an arrangement of tailored subwavelength building blocks from which the material gains unusual macroscopic properties. Nevertheless, these man-made materials often rely on resonating structures, a feature that induces strong energy dissipation losses. More recently, an alternative way has been explored for elastic guided waves. An elastic plate actually supports an ensemble of modes, the so-called Lamb waves, which exhibit complex dispersion properties. Interestingly, some Lamb modes, often referred to as backward modes, display a negative phase velocity [11–14]. This particularity comes from the repulsion between two dispersion branches with close cut-off frequencies, corresponding to a longitudinal and a transverse thickness mode of the same symmetry. The lowest branch exhibits a minimum corresponding to a zero-group velocity (ZGV) point [11,15,16]. This backward mode was the object of several studies. For example, it was shown to be responsible for the backscattering enhancement by shells [17] or negative reflection at a plate edge [18–20]. Then it was taken advantage of to achieve NR at a steplike discontinuity through mode conversion between forward and backward propagating modes (or vice versa) [21,22].

In this paper, we investigate theoretically the conversion of propagating modes at a thickness step to optimize the NR effect. This problem has already been studied for normal [23,24] and oblique incidence [25] at frequencies that only imply low-order modes and do not involve any backward mode. Following the approach of a recent study on negative reflection of Lamb waves at a free plate edge [18], we develop a semianalytical model to calculate the reflection and transmission coefficients between Lamb modes at a symmetric step discontinuity. The optimal parameters (Poisson's ratio, material, thickness ratio) to reach an efficient NR over a broad angular range and a wide frequency bandwidth are then determined using this model. Theoretical results are ultimately confirmed by means of an ultrasound laser experiment performed on a plate of optimal design.

II. DETERMINATION OF THE PLATES MODES

To derive the guided mode equations in the right-handed system (x_1, x_2, x_3), we consider a plate limited by the planes $(x_2 = -h)$ and $(x_2 = h)$ and a wave propagation along the x_1 axis. The displacement field $\boldsymbol{u} = (u_1, u_2, u_3)^T$ and the stress tensor $\boldsymbol{\sigma} = [\sigma_{ij}]$ obeys the elasticity equations given by

$$-\rho\omega^2\boldsymbol{u} = \nabla \cdot \boldsymbol{\sigma}, \tag{1}$$

where ρ is the density of the material and ω is the pulsation. The boundary conditions correspond to the cancellation of the stress tensor on the plate surfaces, $\boldsymbol{\sigma} \cdot \boldsymbol{n} = 0$, where $\boldsymbol{n}$ is the normal to the surface boundary. Solutions are in the form

$$\{u_i(x_1, x_2), \sigma_{ij}(x_1, x_2)\} = \{u_i(x_2), \sigma_{ij}(x_2)\} \cdot e^{(ikx_1)},$$

where k is the wave number. Two sets of solutions satisfy these equations: shear horizontal (SH) modes that are polarized orthogonally to the propagation plane ($u_1 = u_2 = 0$) and Lamb modes, polarized in the propagation plane ($u_3 = 0$). Both families are composed of an infinite number of modes, called propagating, evanescent, or inhomogeneous for a real, pure imaginary, or complex wave number k, respectively. Both Lamb and SH modes can be separated in two independent families of symmetrical and antisymmetrical modes. Symmetric/antisymmetric SH modes correspond to an even/odd $u_3(x_2)$ polarization along the plate thickness. Symmetric/antisymmetric Lamb modes have an even/odd in-plane component $u_1(x_2)$ combined with an odd/even transverse component $u_2(x_2)$. We now briefly recall the equations for SH and Lamb modes that are fully described in various textbooks [26,27].

A. SH modes

The well-known SH mode dispersion relation is

$$\frac{\omega^2}{c_T^2} - k^2 = \left(\frac{n\pi}{2h}\right)^2, \tag{2}$$

with c_T the shear wave velocity and $n = 0, 1, 2....$ The corresponding displacement field is

$$u_3(x_2) = \cos\left(\frac{n\pi}{2h}(x_2 + h)\right).$$

The stress field is then expressed from the displacement field using Eq. (1).

B. Lamb modes

Symmetrical Lamb modes are solutions of the following dispersion relation, often referred to as the Rayleigh-Lamb equation [26,28]:

$$\frac{\omega^4}{c_T^4} = 4k^2q^2\left\{1 - \frac{p}{q}\frac{\tan(ph)}{\tan(qh)}\right\}, \tag{3}$$

with ω the pulsation, $p^2 = \omega^2/c_L^2 - k^2$, $q^2 = \omega^2/c_T^2 - k^2$, c_L the longitudinal wave velocity, c_T the shear wave velocity.

At a fixed pulsation ω, a discrete set of wave numbers k_n satisfy Eq. (3), and only a finite number of propagating modes are supported by the plate, whereas it exists an infinite number of evanescent or inhomogeneous modes. The components of the displacement field for each mode can be expressed as follows [26]:

$$u_1^{(n)}(x_2) = -[k_n \cos(p_n x_2) - R_n q_n \cos(q_n x_2)],$$
$$u_2^{(n)}(x_2) = i[p_n \sin(p_n x_2) + R_n k_n \sin(q_n x_2)],$$

with

$$R_n = \frac{(k_n^2 - q_n^2)\cos(p_n h)}{2k_n q_n \cos(q_n h)}.$$

The stress field can be deduced from $\boldsymbol{u}$ using Eq. (1).

C. Dispersion curves

In the following, we consider a thickness step that is symmetrical with respect to the $x_2 = 0$ plane. Therefore, the reflection/transmission at the step preserves the modes symmetries. As a consequence, a symmetrical Lamb mode is reflected and transmitted into symmetrical Lamb and SH modes. In the following, we only consider symmetrical modes. Figure 1 displays the dispersion curves of the SH and Lamb modes deduced from Eqs. (2) and (3) for a duralumin plate ($\rho = 2790\,\mathrm{kg/m^3}$, $c_L = 6.4\,\mathrm{mm/\mu s}$, $c_T = 3.1\,\mathrm{mm/\mu s}$). The symmetric zero-order Lamb mode S_0 is the extensional mode of the plate. It exhibits free propagation to zero frequency, whereas the higher order modes admit a cutoff frequency. In particular, the S_1 and S_2 modes have cutoff frequencies at $f = c_T/d$ and $f = c_L/2d$, corresponding to shear and longitudinal thickness resonances, respectively. One peculiar property of Lamb waves is the existence of branches for which phase velocity ω/k and group velocity $\partial\omega/\partial k$ are of opposite sign. The corresponding modes, often referred to as backward modes, naturally display a negative phase velocity. They originate from the repulsion between two dispersion branches having close cutoff frequencies, corresponding to a longitudinal and a transverse thickness mode of the same symmetry. This is the case for S_1 and S_2 modes displayed in Fig. 1 in the case of a Duralumin plate. The lowest branch (S_1) exhibits a minimum corresponding to a ZGV point [15,16]. Above this resonance, there is a coexistence of a negative phase velocity (backward) S_{2b} mode and a positive phase velocity (forward) S_1 mode.

III. PROBLEM'S GEOMETRY AND EQUATION SYSTEM

As shown in previous studies [21,22], NR of Lamb waves can be achieved by conversion of a forward mode into a backward mode at a thickness step. Here we consider the conversion between the forward and backward modes S_2 and S_{2b} at a symmetric step [Fig. 2(a)]. Such a geometry is actually optimal for symmetric modes.

To study the interaction of a mode of oblique incidence, a second right-handed system (x_1', x_2, x_3') is introduced [see Fig. 2(a)]. The axis x_3' is oriented along the step interface while the axis x_1' is normal to this step. The thickness is denoted as $d_1 = 2h_1$ for $x_1' < 0$ and $d_2 = 2h_2$ for $x_1' > 0$ with $h_1 > h_2$. We then consider an incident wave coming from the thick part.

Figure 2(b) displays the dispersion curves of the Lamb and SH modes in each part of the plate. Right-going (respectively, left-going) propagating modes correspond to a positive (respectively, negative) group velocity $\partial\omega/\partial k$, whereas the evanescent and inhomogeneous right-going (respectively, left-going) modes correspond to wave numbers with strictly positive (respectively, negative) imaginary parts. Because the dispersion curves scale with the plate thickness [Eqs. (2) and

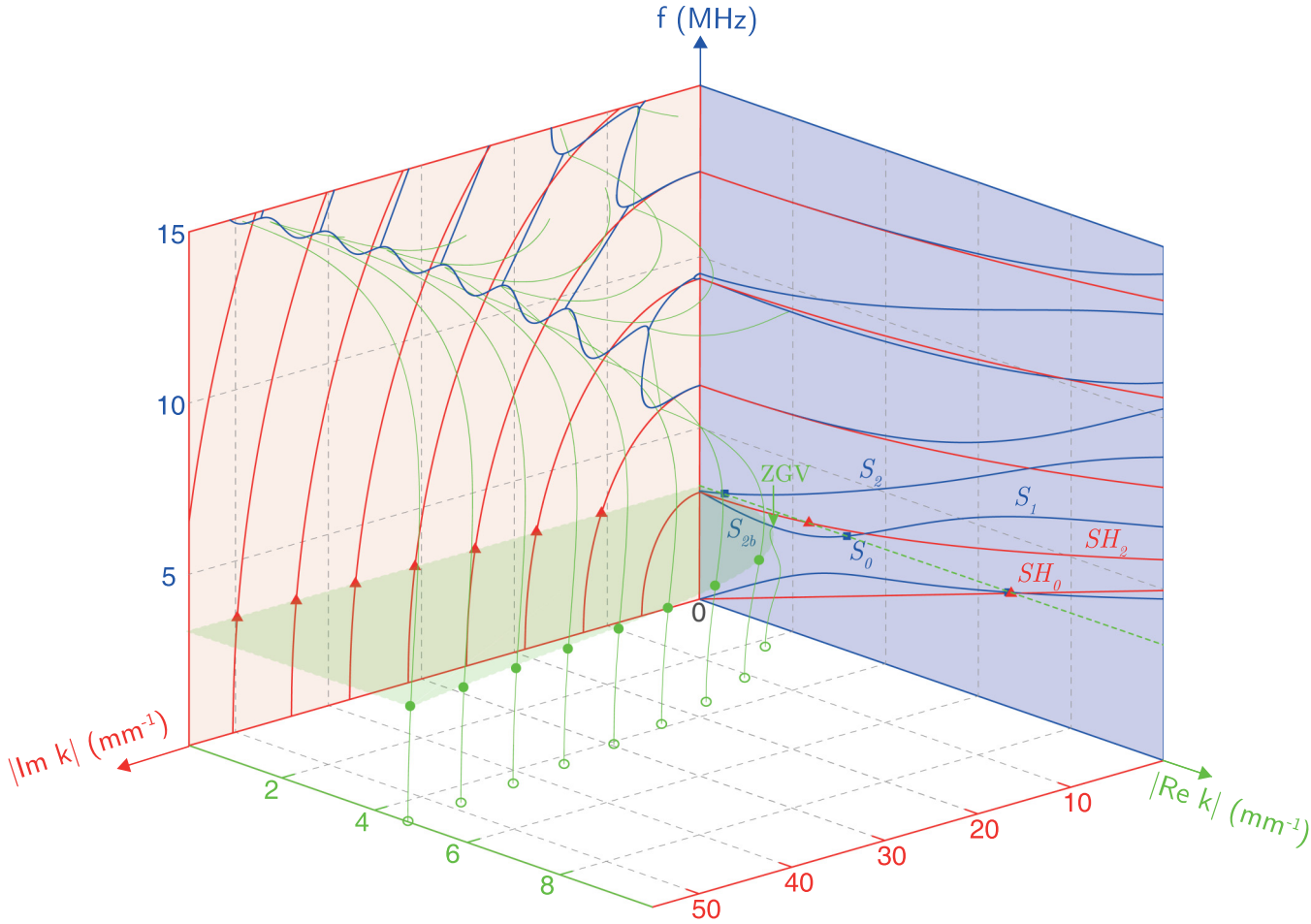

FIG. 1. Dispersion curves of elastic guided modes in a 1-mm thick Duraluminium plate computed from Eqs. (2)–(3): propagating and evanescent SH modes (red), propagating and evanescent Lamb modes (blue), and inhomogeneous Lamb modes (green).

(3)], the forward propagating mode S_2 in the thick part ($x_1' < 0$) crosses the backward-propagating mode S_{2b} in the thin part of the plate. As already observed experimentally [21,22], this crossing point gives rise to NR through an efficient conversion between these two modes at the thickness step. This conversion is now investigated in detail.

Let us consider an incident right-going S_2 mode, of wave number k_I, carrying a unit energy flux toward the step with an angle of incidence θ_I, with respect to the axis (x_1'), as depicted in Fig. 2(a). The corresponding stress displacement field is denoted as $\{u'^I, \sigma'^I\}$. To satisfy the stress-free condition at the interface, this incident Lamb mode is reflected/transmitted into an infinite combination of left-going/right-going Lamb and SH modes of wave numbers $k_{r,n}$ and $k_{t,n}$, respectively. It is necessary to consider not only the propagating modes but also the different evanescent and inhomogeneous Lamb and SH modes [29]. For a given mode n, the reflection and transmission angles, $\theta_{r,n}$ and $\theta_{t,n}$, are determined by the conservation of the wave vector component along x_3', $k_I \sin(\theta_I) = k_{r,n} \sin(\theta_{r,n}) = k_{t,n} \sin(\theta_{t,n})$. The displacement-stress fields, $\{\tilde{u}_i'^{(n)}, \tilde{\sigma}'^{(n)}\}$ and $\{u'^{(n)}, \sigma'^{(n)}\}$, of respectively reflected and transmitted modes expressed in the coordinate system (x_1', x_2, x_3'), can be obtained from the displacement-stress fields $\{u^{(n)}, \sigma^{(n)}\}$ expressed in the coordinate system (x_1, x_2, x_3) using the following equations:

$$\boldsymbol{u}'^{(\boldsymbol{n})} = R(\theta_n) \cdot \boldsymbol{u}^{(\boldsymbol{n})},$$
$$\boldsymbol{\sigma}'^{(\boldsymbol{n})} = R(\theta_n) \cdot \boldsymbol{\sigma}^{(\boldsymbol{n})} \cdot R(\theta_n)^T,$$

where $R(\theta)$ is the rotation matrix,

$$R(\theta) = \begin{bmatrix} \cos(\theta) & 0 & -\sin(\theta) \\ 0 & 1 & 0 \\ \sin(\theta) & 0 & \cos(\theta) \end{bmatrix}.$$

To define transmission and reflection coefficients, it is necessary to normalize each mode so that it carries unit energy flow through the interface:

$$\overline{\boldsymbol{u}}^{(\boldsymbol{n})} = \frac{\boldsymbol{u}^{(\boldsymbol{n})}}{C_n} \quad \text{and} \quad \overline{\boldsymbol{\sigma}}^{(\boldsymbol{n})} = \frac{\boldsymbol{\sigma}^{(\boldsymbol{n})}}{C_n},$$

C_n being the normalization coefficient. To determine this coefficient, we use the biorthogonality relation established by Auld [28], Fraser [30], and generalized by Gunawan and Hirose [31] that involves the biorthogonality coefficient P_{mn}:

$$P_{mn} = \frac{i\omega}{4} \int_{-h}^{+h} \left[u_j'^{(m)} \left(\sigma_{1j}'^{(n)}\right)^* - \left(u_j'^{(n)}\right)^* \sigma_{1j}'^{(m)} \right] dx_2.$$

For propagating modes, the coefficient P_{mn} is nonzero only when $m = n$. The real part of this coefficient corresponds to the energy flow passing through the interface. The coefficient C_n for each propagating mode is thus given by

$$C_n = Re\{P_n\}. \tag{4}$$

For a nonpropagating mode m, the normalization coefficient cannot be expressed using Eq. (4), because the energy flow of this mode is by definition zero through the interface ($\mathrm{Re}\{P_{mm}\} = 0$). However, following Auld's work [28], it exists for each nonpropagating mode m with a wave number k_m a conjugate nonpropagating mode p, associated with a wave number $k_p = k_m^*$. The combination of these modes gives rise to an energy flow given by the real part of P_{mp}. Each nonpropagating mode m can be normalized by the coefficient

$$C_m = \mathrm{Re}\{P_{mp}\},$$

In the following, $\overline{\boldsymbol{u}}$ and $\overline{\boldsymbol{\sigma}}$ will be written as $\boldsymbol{u}$ and $\boldsymbol{\sigma}$ to lighten the expressions.

The boundary conditions at the interface are the stress cancellation on the risers and the displacement and stress continuity on the central part. They can be written as

$$\begin{aligned} u_j^{(I)} + \sum_{n_1=1}^{\infty} r_{(I|n_1)} \tilde{u}_j^{(n_1)} &= \sum_{n_2=1}^{\infty} t_{(I|n_2)} u_j^{(n_2)}, \ |x_2| < h_2, \\ \sigma_{1j}^{(I)} + \sum_{n_1=1}^{\infty} r_{(I|n_1)} \tilde{\sigma}_{1j}^{(n_1)} &= \begin{cases} 0, & h_2 < |x_2| < h_1 \\ \sum_{n_2=1}^{\infty} t_{(I|n_2)} \sigma_{1j}^{(n_2)}, & |x_2| < h_2 \end{cases}, \end{aligned} \tag{5}$$

with $j = 1, 2, 3$. $r_{(I|n)}$ and $t_{(I|n)}$ represent the reflection and transmission coefficients of the incident mode in the nth mode in the corresponding part of the plate. This system of equations cannot be solved analytically and it is necessary to truncate the series and discretize the displacement and stress fields.

IV. INVERSION OF THE PROBLEM

To solve numerically Eqs. (5)–(6), the stress and displacement fields need to be discretized along the normal to the plate with a thickness sampling pitch Δx_2. A maximum number of considered modes is then set by the following spatial Shannon criterion indicating that it is necessary to have at least two points by period:

$$k_{x_2} < \frac{2\pi}{\Delta x_2},$$

with $k_{x_2} = \sqrt{(\omega/c_T)^2 - k^2}$. The number N of selected modes is lower than the number of discrete points along the thickness. This discretization of stress and displacement fields allows us to write Eqs. (5)–(6) in a matrix form:

$$\underbrace{\begin{pmatrix} r_1 \\ \vdots \\ r_i \\ \vdots \\ r_{N_1} \\ t_1 \\ \vdots \\ t_i \\ \vdots \\ t_{N_2} \end{pmatrix}}_{\boldsymbol{C}} = \underbrace{\begin{pmatrix} -\tilde{u}_1^{(1)} & -\tilde{u}_1^{(n)} & -\tilde{u}_1^{(N_1)} & u_1^{(1)} & u_1^{(n)} & u_1^{(N_2)} \\ -\tilde{u}_2^{(1)} & -\tilde{u}_2^{(n)} & -\tilde{u}_2^{(N_1)} & u_2^{(1)} & u_2^{(n)} & u_2^{(N_2)} \\ -\tilde{u}_3^{(1)} & -\tilde{u}_3^{(n)} & -\tilde{u}_3^{(N_1)} & u_3^{(1)} & u_3^{(n)} & u_3^{(N_2)} \\ \cdots & \cdots & & \cdots & \cdots & \\ -\tilde{\sigma}_{11}^{(1)} & -\tilde{\sigma}_{11}^{(n)} & -\tilde{\sigma}_{11}^{(N_1)} & \sigma_{11}^{(1)} & \sigma_{11}^{(n)} & \sigma_{11}^{(N_2)} \\ -\tilde{\sigma}_{12}^{(1)} & -\tilde{\sigma}_{12}^{(n)} & -\tilde{\sigma}_{12}^{(N_1)} & \sigma_{12}^{(1)} & \sigma_{12}^{(n)} & \sigma_{12}^{(2,N_2)} \\ -\tilde{\sigma}_{13}^{(1)} & -\tilde{\sigma}_{13}^{(n)} & -\tilde{\sigma}_{13}^{(N_1)} & \sigma_{13}^{(1)} & \sigma_{13}^{(n)} & \sigma_{13}^{(N_2)} \end{pmatrix}}_{\boldsymbol{M}}^{-1} \cdot \underbrace{\begin{pmatrix} u_1^{(I)} \\ u_2^{(I)} \\ u_3^{(I)} \\ \\ \sigma_{11}^{(I)} \\ \sigma_{12}^{(I)} \\ \sigma_{13}^{(I)} \end{pmatrix}}_{\boldsymbol{Y}}. \tag{7}$$

$\boldsymbol{C}$ is the vector of the reflection and transmission coefficients, $\boldsymbol{M}$ is the matrix containing the displacement-stress field of each mode, and $\boldsymbol{Y}$ is the displacement-stress field of the incident mode. The rectangular matrix $\boldsymbol{M}$ is inverted using a Moore-Penrose pseudoinversion. The chosen sampling interval $\Delta x_2 = 2 \cdot 10^{-4}$ mm implies the consideration of $N_L = 241$ Lamb modes and $N_{\mathrm{SH}} = 120$ SH modes in each part of the plate. This choice is made to fulfill the energy conservation condition with a reasonable precision such that $1 - \sum_{i=1}^{N} (|r_i|^2 + |t_i|^2) < 10^{-3}$.

V. OPTIMIZATION OF THE NEGATIVE REFRACTION PHENOMENON

This semianalytical model is first used to determine the thickness ratio that maximizes the conversion between the forward mode S_2 and the backward one S_{2b} at normal incidence.

Figure 3(a) displays the transmission coefficient $|t_{S_2 \to S2b}|$ at normal incidence for various materials as a function of the thickness ratio d_2/d_1. For each thickness ratio, the amplitude transmission coefficient is calculated at the crossing frequency, intersection of S_2 mode in the thick part and S_{2b} mode

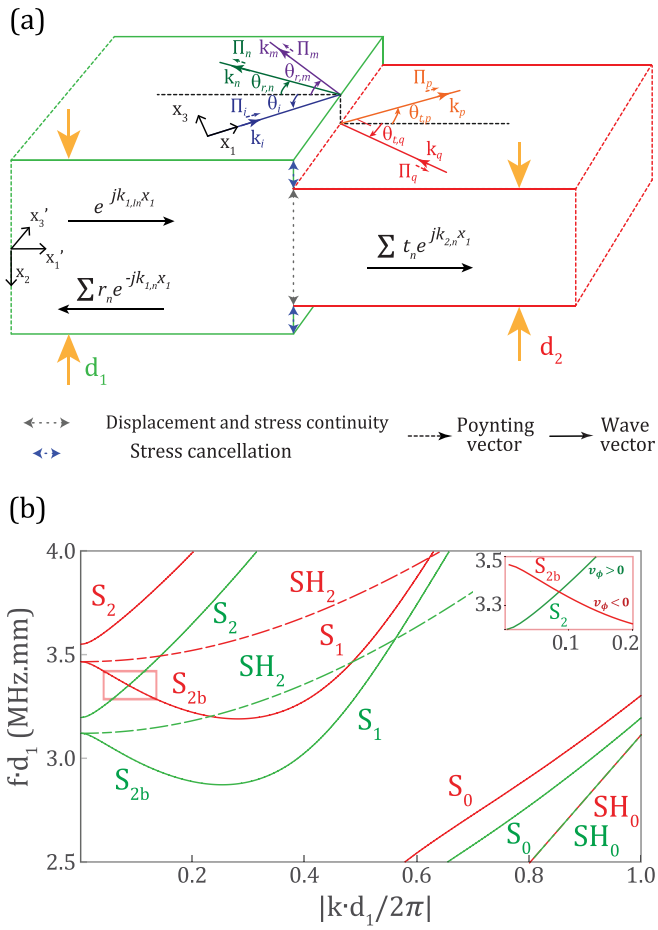

FIG. 2. (a) Geometry of the problem that shows the interaction of a Lamb mode with a step interface. To satisfy the continuity equations at the interface, the incident wave is transmitted and reflected into an infinite combination of Lamb and SH modes. (b) Lamb and SH propagating mode dispersion curves in both parts of the plate (green for $d_1 = 1$ mm and red for $d_2 = 0.9$ mm). The forward propagating mode S_2 in the thick part intersects the backward propagating mode S_{2b} in the thin part.

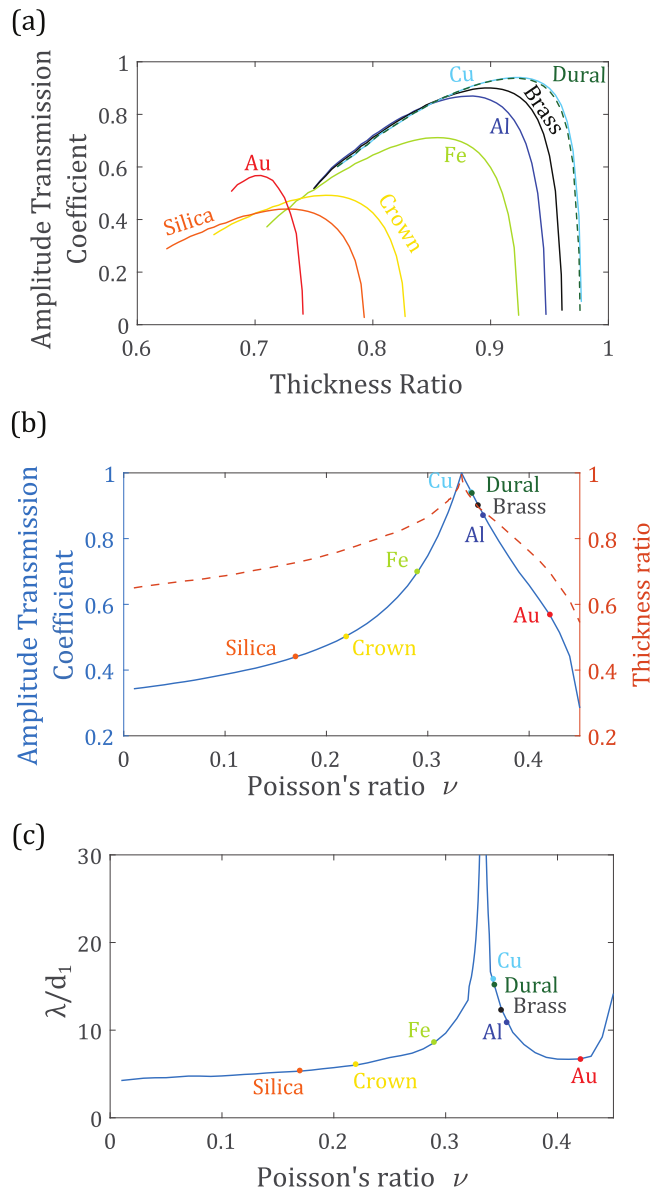

FIG. 3. Transmission of the S_2 mode at normal incidence: (a) Transmission coefficient $|t_{S_2 \to S_{2b}}|$ as a function of the thickness ratio d_2/d_1 for different materials. (b) Amplitude transmission coefficient (continuous line) and the associated best thickness ratio (dotted line) as a function of the Poisson's ratio. The coefficient reaches 1 for $\nu = 1/3$, that is to say when S_2 and S_{2b} share the same cutoff frequency. (c) Evolution of the crossing wavelength as a function of the Poisson's ratio.

in the thin part [see Fig. 2(b)]. Interestingly, the amplitude transmission coefficient can be close to unity for materials such as Duralumin or copper. This can be explained by the close displacement profiles of the two modes at the crossing frequency [see Fig. 4(b)]. However, for each material, the amplitude transmission coefficient strongly decreases when the thickness ratio tends towards unity. In that asymptotic case, the crossing frequency approaches the cutoff frequencies where the S_2 mode tends to be purely longitudinal while the S_{2b} mode becomes purely shear. An important mode mismatch is thus found when $d_2/d_1 \to 1$ [see Fig. 4(a)]. Figure 3(b) displays $|t_{S_2 \to S2b}|$ and the optimum thickness ratio as a function of the Poisson's ratio ν. Interestingly, when ν tends to the value $1/3$, the amplitude transmission coefficient reaches unity with an optimum thickness ratio of 1. This critical value of ν indeed implies the coincidence of S_2 and S_{2b} cutoff frequencies. S_2 and S_{2b} modes are thus strictly identical in that case, which means a full mode overlap and a perfect conversion between them [see Fig. 4(c)]. Such case has been recently investigated by Stobbe and Murray [32] as it also gives rise to a Dirac cone in the dispersion curves. This means that the group velocity remains finite while the wave number tends to zero. However, in the present case, an infinite wavelength limits the experimental interest for this ideal case. A compromise thus has to be found between the transmission coefficient and the mode wavelength and, in that respect, the choice of Duralumin appears to be optimal: The transmission coefficient reaches $|t_{S_2 \to S2b}| = 0.94$ for a thickness ratio d_2/d_1 of 0.92 and a reasonable wavelength $\lambda = 13.3 d_1$. Moreover, Duralumin has a much lower absorption coefficient than copper (∼1 dB/m for Duralumin and in that respect, ∼20 dB/m for copper [33]).

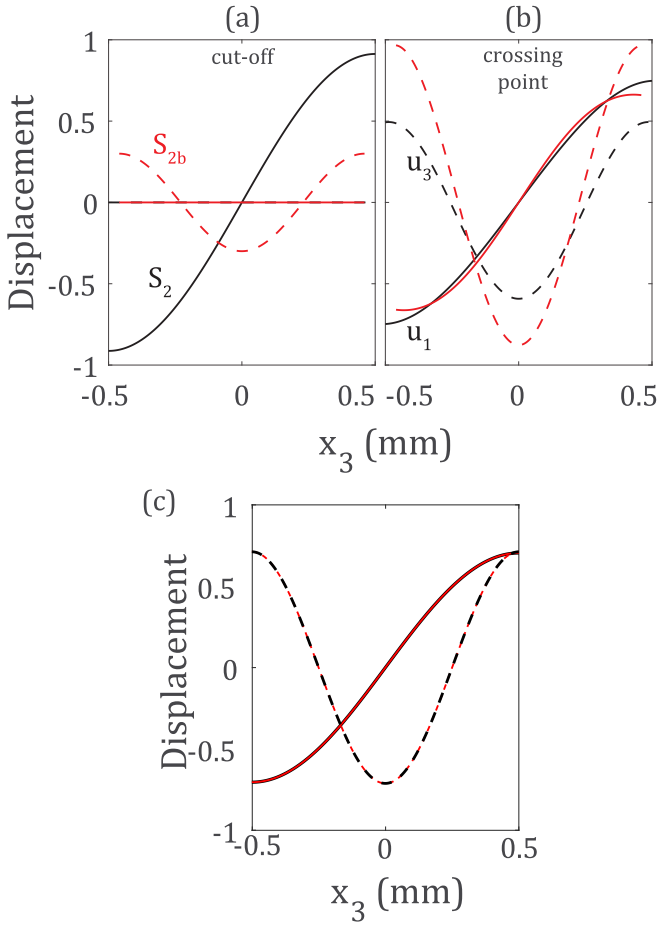

FIG. 4. Displacement u_3 (continuous line) and u_1 (dotted line) of S_2 (black) and S_{2b} (red) in a 1-mm thick Duralumin plate (a) at the cutoff frequency, (b) at the crossing point, and (c) at the coincidence when $\nu = 1/3$.

Now that the Duralumin has been chosen, we investigate the bandwidth over which the conversion between S_2 and S_{2b} remains efficient. The frequency dependence of $|t_{S_2 \to S2b}|$ is displayed in Fig. 5(a). The NR of Lamb waves appears to be broadband: for $d_1 = 1$mm, the transmission coefficient is above 0.9 over a frequency bandwidth $\Delta f \sim 0.15$ MHz. The NR phenomenon can thus be observed in the time domain for wave packets of length $\Delta t \sim 1/\Delta f \sim 6$ μs. This important feature will be confirmed experimentally in the next section.

The angular dependence of the NR phenomenon is also particularly important for the implementation of a flat lens. Figure 5(b) displays the reflection and transmission coefficients for the various propagating modes supported by each part of the plate for an incident S_2 mode. It appears that $|t_{S2->S2b}|$ remains above 0.8 over an angular range of 45°. Note that, for large angles of incidence, the S_2 mode is mainly reflected into itself and the SH_2 mode. As we will see now, this angular robustness of the $S_2 \to S_{2b}$ conversion ensures a large aperture angle for the NR flat lens.

VI. NEGATIVE REFRACTION LENS

The NR flat lens is now experimentally and theoretically investigated. It consists of a plate with two symmetrical steps.

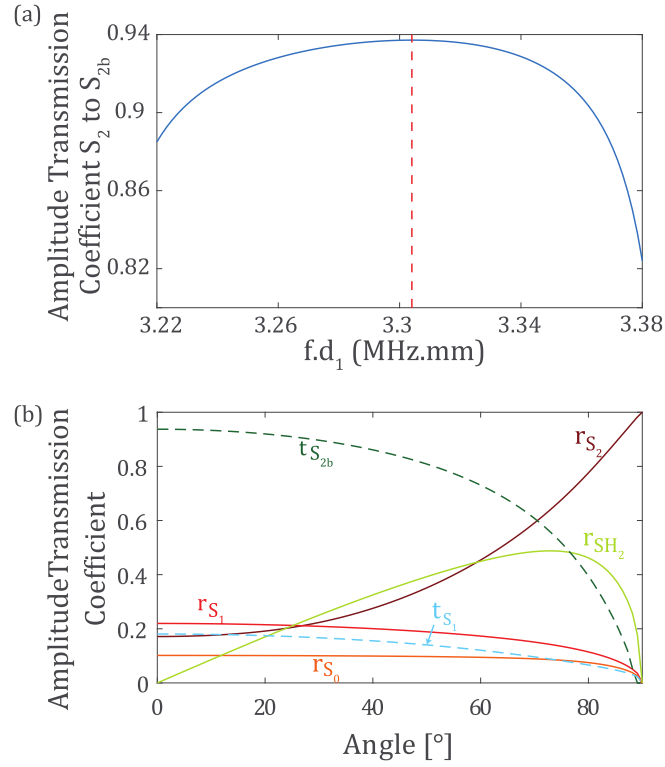

FIG. 5. (a) Variation of the amplitude transmission coefficient at the optimum thickness ratio as a function of frequency. (b) Reflection and transmission coefficients as a function of the S_2-mode incident angle at frequency $f = 3.33$ MHz. (The S_2 to SH_0 reflection coefficient and the transmission ones to S_0 and SH_0 are not shown here because smaller than 10^{-3}).

For the experiment, we engraved a 1-mm-thick Duralumin plate by chemical erosion using iron chloride to obtain a 0.9-mm thick thin part of length $d = 50$ mm [see Fig. 6 (a)]. The plate dimensions (200 × 200 mm) are chosen to limit reflections at the edges during the recording. To measure the wave field induced by an axisymmetric source in the flat lens, one can use a transducer as a source, and measure the normal displacement at every point using an heterodyne interferometer. However, because the optical reflectivity in the eroded part is low, the normal displacement is underestimated by the interferometer. To overcome this issue, we take advantage of spatial reciprocity and use a laser source while measuring the normal displacement with the transducer. The excitation of the plate is then achieved over a grid of points that maps 150 × 50 mm^2 of the plate surface [see Fig. 6(a)] with a 1-mm pitch using a 1064-nm pulsed Nd:YAG laser (Centurion, Quantel). The out-of-plane displacement is measured with a 10-mm-diameter transducer (Olympus V183-RM) glued with phenyl salicylate on the thick part and placed at a distance $D = 25$ mm from the first step [see Fig. 6(a)]. Signals detected by the transducer are fed into a high-speed usb oscilloscope (TiePie HS5) and transferred to a computer. A spatiotemporal discrete Fourier transform (DFT) of the recorded wave fronts is then performed from 3.22 to 3.52 MHz and for spatial frequencies $k/(2\pi)$ ranging from -0.15 to 0.15 mm^{-1}. To avoid reflections on the free edges of the plates, the DFT is calculated for adapted time windows in each part of the lens:

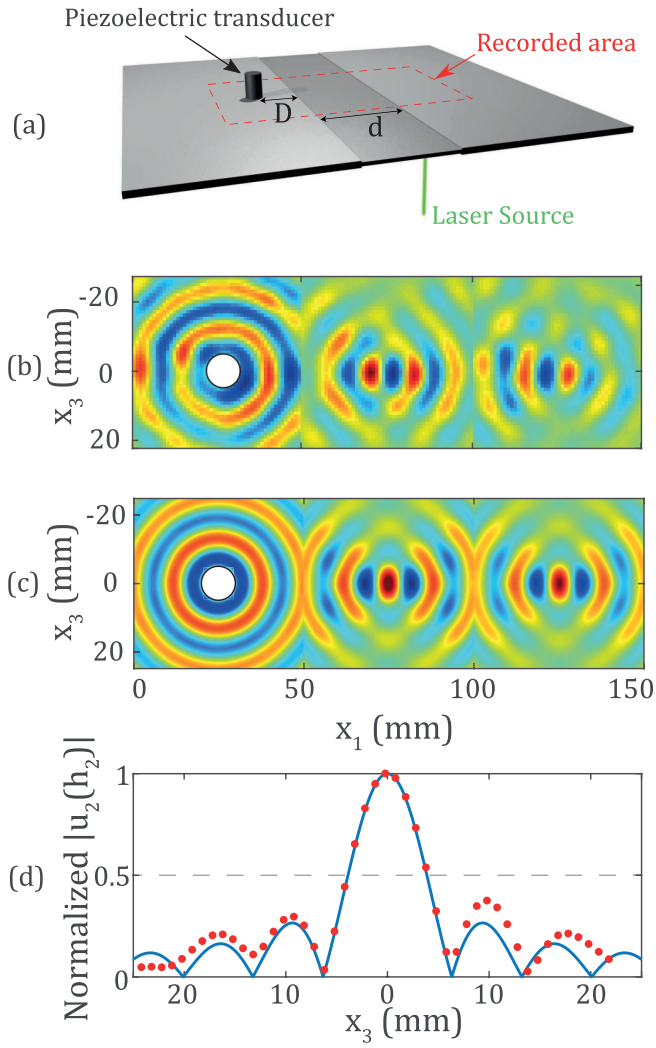

FIG. 6. Wave-field associated with the S_2 and S_{2b} modes supported by the NR lens made of a Duralumin plate with a thickness ratio d_2/d_1 of 0.9. (a) Experimental setup, $D = 25$ mm. (b) Experimental result obtained with the laser source. (c) Semianalytical result. (d) Transverse focusing in the thin part of the plate: Measured normal displacement (red disks) are compared to semi-analytical predictions (continuous blue line).

$0 - 20$ μs for the first thick part, $10 - 70$ μs for the thin part and $40 - 100$ μs for the second thick part.

Figure 6(b) shows the normal displacement field measured on the plate at the frequency $f = 3.33$ MHz. As predicted theoretically [Fig. 5(b)], the NR lens shows remarkable focusing capabilities with a large angular aperture. The behavior of the plate lens can also be observed in the time domain [22]. Due to the spectral robustness of the $S_2 \rightarrow S_{2b}$ conversion [Fig. 5(a)], the plate lens also operates for wave packets of finite duration (6 μs). The result is displayed in the Supplemental movie [34].

To go beyond a qualitative analysis, we now quantitatively compare experiment and theory. To that aim, the semianalytical model is used to calculate the wave field induced by an axisymmetric source in the NR lens (see Supplemental Material for the detailed method [34]). To mimic the experiment and to account for the duration of the recording, only angles up to 60° have been considered. The obtained displacement field is displayed in Figure 6(c). It displays an excellent qualitative agreement with the experiment [Fig. 6(b)].

For a quantitative comparison, two relevant observables are evaluated. The first is the ratio between the maximum displacement on the focal spot in the third and second part of the plate. This ratio is of 0.84, experimentally, while it is of 0.87 using the semianalytical model. The second is the full width at half maximum (FWHM) of the focal spot in the thin part of the plate along the x_3 direction. The corresponding experimental and theoretical focal spots are compared in Fig. 6(d). Experimentally, a FWHM of 7.9 mm is found, while theory predicts a FWHM of 7.8 mm. Those observables show a remarkable quantitative agreement. The residual discrepancy can be explained by small experimental imperfections. First, the step is not perfectly abrupt. Second, the thickness of the thin part of the plate shows some small variation (between 0.88 mm and 0.92 mm), leading to shifting the crossing point between S_2 and S_{2b}. At last, albeit weak, the attenuation of Lamb modes is also increased by the leakage in the air ($<$1dB/m).

VII. CONCLUSION

A semianalytical model to study the interaction of Lamb waves with a steplike thickness was presented. The conversion between forward and backward Lamb modes associated with NR was analyzed. The semianalytical model allows us to investigate this phenomenon by computing the transmission and reflection coefficient as a function of Poisson's ratio, thickness ratio, angle of incidence, and frequency. Thus an optimal design to achieve negative refraction is found. This semianalytical model evaluates the frequency and angular robustness of the NR process. It shows that a Duraluminium plate, as used in previous works [15,22], displays adequate mechanical properties to observe NR. Relying on these results, we have designed and tested a NR lens effective in the time domain. The wave field recorded by means of laser ultrasonic techniques is in quantitative agreement with our theoretical prediction. The perspective of this paper was to investigate NR-related phenomena such as the notion of complementary media [35] and the ability to cancel the propagation of waves by adjoining two mirror regions of opposite refractive indices. Beyond NR, the proposed theoretical model is much more general and can be applied to other types of discontinuity and Lamb modes. Another perspective could be the consideration of evanescent or inhomogeneous Lamb modes in the model to implement a superlens for Lamb waves.

ACKNOWLEDGMENTS

The authors are grateful for funding provided by the Agence Nationale de la Recherche (No. ANR-15-CE24-0014-01, Research Project COPPOLA)and by LABEX WIFI (Laboratory of Excellence within the French Program Investments for the Future, No. ANR-10-LABX-24 and No. ANR-10-IDEX-0001-02 PSL*). B.G. acknowledges financial support from the French Direction Générale de l'Armement (DGA).

[1] J. B. Pendry, Negative Refraction Makes a Perfect Lens, Phys. Rev. Lett. **85**, 3966 (2000).

[2] V. G. Veselago, The electrodynamics of substances with simultaneously negative values of epsilon and mu, Phys. Usp. **10**, 509 (1968).

[3] N. Fang, H. Lee, C. Sun, and X. Zhang, Sub–diffraction-limited optical imaging with a silver superlens, Science **308**, 534 (2005).

[4] U. Leonhardt, Optical conformal mapping, Science **312**, 1777 (2006).

[5] J. B. Pendry, Negative refraction, Contemp. Phys. **45**, 191 (2004).

[6] B. Morvan, A. Tinel, A.-C. Hladky-Hennion, J. Vasseur, and B. Dubus, Experimental demonstration of the negative refraction of a transverse Elastic wave in a two-dimensional solid phononic crystal, Appl. Phys. Lett. **96**, 101905 (2010).

[7] C. Croënne, E. Manga, B. Morvan, A. Tinel, B. Dubus, J. Vasseur, and A.-C. Hladky-Hennion, Negative refraction of longitudinal waves in a two-dimensional solid-solid phononic crystal, Phys. Rev. B **83**, 054301 (2011).

[8] J. Pierre, O. Boyko, L. Belliard, J. Vasseur, and B. Bonello, Negative refraction of zero order flexural Lamb waves through a two-dimensional phononic crystal, Appl. Phys. Lett. **97**, 121919 (2010).

[9] M. Dubois, M. Farhat, E. Bossy, S. Enoch, S. Guenneau, and P. Sebbah, Flat lens for pulse focusing of elastic waves in thin plates, Appl. Phys. Lett. **103**, 071915 (2013).

[10] R. Zhu, X. N. Liu, G. K. Hu, C. T. Sun, and G. L. Huang, Negative refraction of elastic waves at the deep-subwavelength scale in a single-phase metamaterial, Nat. Commun. **5**, 5510 (2014).

[11] I. Tolstoy and E. Usdin, Wave propagation in elastic plates: low and high mode dispersion, J. Acoust. Soc. Am. **29**, 37 (1957).

[12] R. D. Mindlin, Waves and vibrations in isotropic elastic plates, *Structural Mechanics* (Pergamon Press, New York, 1960), pp. 199–232.

[13] A. H. Meitzler, Backward-wave transmission of stress pulses in elastic cylinders and plates, J. Acoust. Soc. Am. **38**, 835 (1965).

[14] K. Negishi, Existence of negative group velocities in Lamb waves, Jpn. J. Appl. Phys. **26**, 171 (1987).

[15] C. Prada, O. Balogun, and T. Murray, Laser-based ultrasonic generation and detection of zero-group velocity Lamb waves in thin plates, Appl. Phys. Lett. **87**, 194109 (2005).

[16] S. D. Holland and D. E. Chimenti, Air-coupled acoustic imaging with zero-group-velocity Lamb modes, Appl. Phys. Lett. **83**, 2704 (2003).

[17] G. Kaduchak, D. H. Hughes, and P. L. Marston, Enhancement of the backscattering of high-frequency tone bursts by thin spherical shells associated with a backwards wave: Observations and ray approximation, J. Acoust. Soc. Am. **96**, 3704 (1994).

[18] B. Gérardin, J. Laurent, C. Prada, and A. Aubry, Negative reflection of Lamb waves at a free edge: Tunable focusing and mimicking phase conjugation, J. Acoust. Soc. Am. **140**, 591 (2016).

[19] M. Germano, A. Alippi, A. Bettucci, and G. Mancuso, Anomalous and negative reflection of Lamb waves in mode conversion, Phys. Rev. B **85**, 012102 (2012).

[20] B. Gérardin, J. Laurent, F. Legrand, C. Prada, and A. Aubry, Negative reflection of elastic guided waves in chaotic and random scattering media, arXiv:1710.06150 [Sci. Rep. (to be published)].

[21] S. Bramhavar, C. Prada, A. A. Maznev, A. G. Every, T. B. Norris, and T. W. Murray, Negative refraction and focusing of elastic Lamb waves at an interface, Phys. Rev. B **83**, 014106 (2011).

[22] F. D. Philippe, T. W. Murray, and C. Prada, Focusing on plates: Controlling guided waves using negative refraction, Sci. Rep. **5**, 11112 (2015).

[23] C. Schaal and A. Mal, Lamb wave propagation in a plate with step discontinuities, Wave Motion **66**, 177 (2016).

[24] B. Poddar and V. Giurgiutiu, Scattering of Lamb waves from a discontinuity: An improved analytical approach, Wave Motion **65**, 79 (2016).

[25] F. Feng, Z. Shen, and J. Shen, Scattering of obliquely incident waves by straight features in a plate, Wave Motion **60**, 84 (2016).

[26] D. Royer and E. Dieulesaint, *Elastic Waves in Solid* (Springer Verlag, Berlin, 2000), Vol. 1.

[27] J. D. Achenbach, *Wave Propagation in Elastic Solids* (North-Holland, Amsterdam, 1980).

[28] B. A. Auld, *Acoustic Fields and Waves in Solids* (John Wiley and Sons, New York, 1973).

[29] S. F. Morse and P. L. Marston, Meridional ray backscattering enhancements for empty truncated tilted cylindrical shells: Measurements, ray model, and effects of a mode threshold, J. Acoust. Soc. Am. **112**, 1318 (2002).

[30] W. Fraser, Orthogonality relation for the Rayleigh–Lamb modes of vibration of a plate, J. Acoust. Soc. Am. **59**, 215 (1976).

[31] A. Gunawan and S. Hirose, Reflection of obliquely incident guided waves by an edge of a plate, Mater. Tran. **48**, 1236 (2007).

[32] D. M. Stobbe and T. W. Murray, Conical dispersion of Lamb waves in elastic plates, Phys. Rev. B **96**, 144101 (2017).

[33] C. Prada, D. Clorennec, and D. Royer, Power law decay of zero group velocity Lamb modes, Wave Motion **45**, 723 (2008).

[34] See Supplemental Material at http://link.aps.org/supplemental/10.1103/PhysRevB.98.214114 for videos of the negative refraction in time domain for numerical and experimental results.

[35] J. B. Pendry and S. A. Ramakrishna, Focusing light using negative refraction, J. Phys.: Condens. Matter. **15**, 6345 (2003).